Title
Role of the reaction of stabilized Criegee intermediates with peroxy radicals in particle formation and growth in air

Journal
Physical Chemistry Chemical Physics, 17(19)

ISSN
0956-5000

Authors
Zhao, Yue
Wingen, Lisa M
Perraud, Véronique
et al.

Publication Date
2015-05-21

DOI
10.1039/c5cp01171j

PCCP

PAPER

View Article Online
View Journal | View Issue

Cite this: *Phys. Chem. Chem. Phys.*, 2015, **17**, 12500

Role of the reaction of stabilized Criegee intermediates with peroxy radicals in particle formation and growth in air†

Yue Zhao, Lisa M. Wingen, Véronique Perraud, John Greaves and Barbara J. Finlayson-Pitts*

Received 26th February 2015,
Accepted 14th April 2015

DOI: 10.1039/c5cp01171j

www.rsc.org/pccp

Ozonolysis of alkenes is an important source of secondary organic aerosol (SOA) in the atmosphere. However, the mechanisms by which stabilized Criegee intermediates (SCI) react to form and grow the particles, and in particular the contributions from oligomers, are not well understood. In this study, ozonolysis of *trans*-3-hexene (C_6H_{12}), as a proxy for small alkenes, was investigated with an emphasis on the mechanisms of particle formation and growth. Ozonolysis experiments were carried out both in static Teflon chambers (18–20 min reaction times) and in a glass flow reactor (24 s reaction time) in the absence and presence of OH or SCI scavengers, and under different relative humidity (RH) conditions. The chemical composition of polydisperse and size-selected SOA particles was probed using different mass spectrometric techniques and infrared spectroscopy. Oligomers having SCI as the chain unit are found to be the dominant components of such SOA particles. The formation mechanism for these oligomers suggested by our results follows the sequential addition of SCI to organic peroxy (RO_2) radicals, in agreement with previous studies by Moortgat and coworkers. Smaller particles are shown to have a relatively greater contribution from longer oligomers. Higher O/C ratios are observed in smaller particles and are similar to those of oligomers resulting from RO_2 + *n*SCI, supporting a significant role for longer oligomers in particle nucleation and early growth. Under atmospherically relevant RH of 30–80%, water vapor suppresses oligomer formation through scavenging SCI, but also enhances particle nucleation. Under humid conditions, or in the presence of formic or hydrochloric acid as SCI scavengers, peroxyhemiacetals are formed by the acid-catalyzed particle phase reaction between oligomers from RO_2 + *n*SCI and a *trans*-3-hexene derived carbonyl product. In contrast to the ozonolysis of *trans*-3-hexene, oligomerization involving RO_2 + *n*SCI does not appear to be prevalent in the ozonolysis of α-cedrene ($C_{15}H_{24}$), indicating different particle formation mechanisms for small and large complex alkenes that need to be taken into account in atmospheric models.

Introduction

Organic aerosol makes up a substantial fraction (20–90%) of submicron particles in the atmosphere,[1–3] of which up to 90% is secondary organic aerosol (SOA).[2,4] SOA is produced by atmospheric oxidation of volatile organic compounds (VOCs) that can lead to the formation of products having sufficiently low vapor pressures to either nucleate to form new particles or condense onto pre-existing particles.[5,6] At present, however, a quantitative understanding of SOA formation from such oxidation processes remains limited, resulting in large uncertainties in predicting the impacts of organic aerosol on air quality, climate and human health.[1–3,7–9]

Ozonolysis of alkenes is an important source of SOA in the atmosphere.[1,5,6,10,11] Ozone–alkene reactions are known to proceed *via* the formation of a primary ozonide which decomposes to a carbonyl product and a biradical/zwitterion known as the Criegee intermediate.[5,6,10] Over the past decades, special attention has been given to the ozonolysis of large biogenic VOCs such as monoterpenes and sesquiterpenes,[1,3,10] which have structures and large molecular masses that favor the formation of low volatility products upon atmospheric oxidation. Recently, high molecular weight oligomers have been recognized as major constituents of SOA from ozonolysis of large alkenes ($\geq C_{10}$).[1,12–18] However, the identity of these oligomers and their formation mechanisms are not well understood. Several pathways leading to oligomer formation have

Department of Chemistry, University of California, Irvine, CA, 92697, USA. E-mail: bjfinlay@uci.edu; Fax: +1-949-824-2420; Tel: +1-949-824-7670

† Electronic supplementary information (ESI) available. See DOI: 10.1039/c5cp01171j

been suggested, including (i) reactions of stabilized Criegee intermediates (SCI) with carboxylic acids and carbonyls, forming α-acyloxy hydroperoxides and secondary ozonides, respectively;[12,15,18–20] (ii) reactions of monomer products from ozonolysis, *e.g.*, aldol condensation, peroxyhemiacetal formation, gem-diol formation, esterification, acetal and hemiacetal formation;[13,16,18,21–26] and (iii) formation of non-covalently bound dimer clusters of carboxylic acids.[21,26–28] Pathway (i) is thought to take place in the gas phase, and pathway (ii) is suggested to occur mainly on the surface or within the bulk of SOA particles, whereas pathway (iii) may occur in both phases. Quite recently, gas phase formation of esters[17] and highly oxidized products (termed extremely low-volatility organic compounds, ELVOCs)[29–32] have been suggested in the α-pinene/O_3 system. The formation of ELVOCs possibly involves intramolecular isomerization of RO_2 radicals.[30,32–35]

Formation of oligomers has also been reported for ozonolysis of small alkenes ($<C_6$).[40–44] For example, chamber studies of ozonolysis of isoprene have shown the formation of oligomers in SOA through interspecies reactions of small oxidation products such as aldehydes and carboxylic acids in the condensed phase, including through aldol condensation, hemiacetal formation, and esterification.[40,41] Accurate mass measurements suggested that these oligomers have high oxygen content (average O/C = 0.6) and comprise the majority of isoprene/O_3 derived SOA.[40] Recently, theoretical[45,46] and experimental[41–44] studies have suggested the gas phase formation of low-volatility oligomers containing SCI as the repeat unit during the ozonolysis of small enol ethers and alkenes (including isoprene) in dry air. Two different mechanisms have been proposed: sequential addition of SCI to peroxy radicals (RO_2) (reaction (R1)),[43] or to hydroperoxides (ROOH) (reaction (R2)).[44]

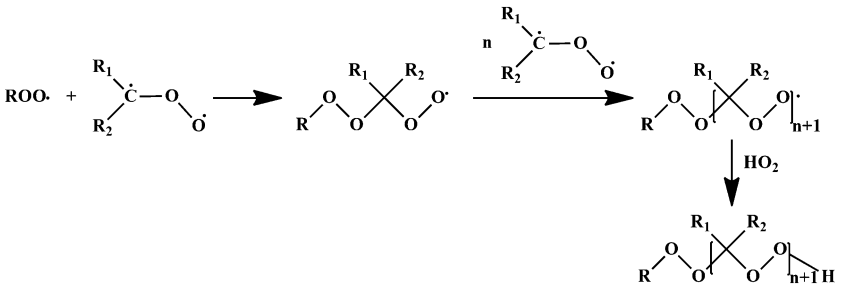

There is growing evidence that oligomers play a key role in initial particle formation from large alkenes because of their predicted very low vapor pressures.[19,36] In ozonolysis experiments where SCI were scavenged using small acids or water, particle nucleation was shown to be suppressed, suggesting that the oligomers formed from SCI were potentially the nucleating precursors.[19,20,37] In an α-pinene/O_3 system, the formation of 10–20 nm particles was well correlated with gas phase oxidation products of high molecular weight (MW) (430–560 Da), whereas particles larger than 20 nm were correlated with those having lower MW (140–380 Da).[31] In a similar system, the gas phase formation of high MW ester dimers was shown to be correlated with new particle formation in the presence of inorganic seed particles.[17] In another study, ELVOCs, which have been detected in both chamber experiments and ambient air,[29–32] were suggested to be capable of acting as nano-condensation nuclei and driving the formation of 3 nm particles.[30] It has also been demonstrated, by measuring the composition of α-pinene/O_3 SOA particles using mass spectrometry, that smaller particles contain more higher MW components[38] and lower volatility carboxylic acids,[39] than do larger particles. This is consistent with the role of oligomers in the initial stages of particle formation.

Sadezky *et al.*[43] investigated the formation of oligomers from the ozonolysis of a number of simple alkenes including *trans*-3-hexene in a static chamber, and proposed the structures and mechanisms shown in reaction (R1). We report here an expanded investigation of the ozonolysis of *trans*-3-hexene in which particle composition is probed as a function of size. In addition, the influence of water vapor, OH and SCI scavengers, as well as the phase state of SOA particles (which plays critical roles in various physical and chemical processes of aerosols)[47–56] are elucidated and possible mechanisms are examined in light of predictions of a box model for this system. Initial studies of the ozonolysis of the much larger and complex biogenic alkene α-cedrene are also reported, and it is shown that the mechanism of particle formation for this sesquiterpene is different from that for *trans*-3-hexene. These results have important implications for modeling particle formation and growth in air from alkene ozonolysis.

Experimental

Apparatus

Ozonolysis experiments were conducted both in a flow reactor and in static chambers in the absence and presence of an OH or

SCI scavenger at 295 ± 1 K. Experiments on the effects of relative humidity (RH) were carried out in the static chamber.

Flow reactor. The major section of the reactor consisted of a 4.6 cm i.d. and 85 cm long quartz tube. Two end caps were mated to the tube and sealed with O-rings. Gas phase *trans*-3-hexene was generated by using an automated syringe pump (Pump Systems Inc., model NE-1000) to inject the pure liquid (Sigma-Aldrich, >99%) into 3.36 L min^{-1} dry air (Praxair, Ultra zero air). The air flow containing *trans*-3-hexene was introduced concentrically into the reactor through the upstream end cap. Ozone, produced by flowing O_2 (Praxair, Ultra High Purity, 99.993%) at 0.24 L min^{-1} through a pen-ray mercury lamp (model 11SC-2), was sent to the flow reactor just downstream of the *trans*-3-hexene inlet through a perforated glass tube in the radial direction. The O_3 concentration was measured using a UV-vis spectrometer (Ocean Optics, HR4000). The total flow rate in the reactor was 3.6 L min^{-1}, giving a residence time of 24 s. The typical initial concentrations of *trans*-3-hexene and O_3 in the flow reactor were 12.5 ppm and 13 ppm, respectively. In some experiments, ~6500 ppm of cyclohexane (Fisher Scientific, 99.99%) or ~1800 ppm of chlorocyclohexane (Sigma-Aldrich, 99%) were added, using the same method as for *trans*-3-hexene, to the flow reactor as a scavenger for OH formed from ozonolysis.

At the outlet of the flow reactor, size distributions of SOA particles were measured using a scanning mobility particle sizer (SMPS, TSI), which consists of an electrostatic classifier (model 3080), a long differential mobility analyzer (DMA, 3081) and a condensation particle counter (model 3776). In addition, the polydisperse particles exiting the flow reactor were collected on a 37 mm quartz filter at a flow rate of 3.4 L min^{-1} for 60 min, with venting of the remaining flow at 0.2 L min^{-1} to the hood. Excellent collection efficiency (>99%) was obtained for particles of all diameters by measuring particles downstream of the filter using the SMPS. After collection, the filters were immediately extracted with 2 mL acetonitrile (Fisher Scientific, 99.9%) by sonicating for 12 min. The resulting solutions were analyzed using an LCT Premier electrospray ionization time-of-flight mass spectrometer (ESI-MS, Waters). In order to explore the size-dependence of the composition, monodisperse particles of different sizes (50, 75, 80, 100, 150, and 200 nm) were selected using the DMA, and then either measured online using a high resolution time-of-flight aerosol mass spectrometer (HR-ToF-AMS, Aerodyne) or collected onto a quartz filter for offline ESI-MS measurements. It should be noted that larger, multiply charged particles could also contribute in these size-selection experiments due to their equivalent electrical mobility.

To compare the particle formation mechanisms between small simple and large complex alkenes, flow reactor experiments were also conducted to investigate α-cedrene ozonolysis in the absence and presence of cyclohexane, using the same experimental procedures as those for *trans*-3-hexene ozonolysis. The initial concentrations of α-cedrene (Sigma-Aldrich, 98.0%), O_3 and cyclohexane (when used) were 500 ppb, 16 ppm, and 262 ppm, respectively. The reaction time was 30 s. The polydisperse SOA particles formed in the reactor were collected onto a 47-mm PTFE filter (Millipore Fluoropore, 0.45 μm pore size) for ESI-MS analysis.

Chamber. Two types of chamber experiments were carried out: (i) ozonolysis of *trans*-3-hexene in the absence and presence of formic acid or hydrochloric acid (HCl) as an SCI scavenger in a 300 L Teflon chamber and (ii) ozonolysis of *trans*-3-hexene at lower concentrations and different RH in a 450 L Teflon chamber. Formic acid was added by injecting a known volume of liquid (Sigma-Aldrich, ≥95%) into the chamber. The HCl solution (37% wt, J.T. Baker) was freeze–pump–thawed and the headspace above the solution on warming expanded into a separate bulb, the contents of which were flushed into the chamber. The vapor in the headspace above such a solution at 293 K is comprised of ~97% HCl and ~3% water by volume.[57] Water vapor was added by bubbling air through nanopure water into the chamber. *trans*-3-Hexene was then added by injecting a defined volume of pure liquid into the chamber. After 10 min to allow for the evaporation of *trans*-3-hexene and mixing of the gases, O_3 produced by a commercial ozone generator (Polymetrics, Model T-816) was added to the chamber to initiate the reaction. Type (i) experiments were performed with initial *trans*-3-hexene and O_3 concentrations of 10 ppm each, and formic acid concentrations of 0–6 ppm and HCl concentrations of 0–30 ppm. Type (ii) experiments were performed at an initial *trans*-3-hexene concentration of 800 ppb and an O_3 concentration of 1.5 ppm in the RH range of 0–80%, which was monitored using a humidity probe (Vaisala, HMT 234).

The size distribution of SOA particles formed in the chamber was measured using SMPS. After an 18 min reaction, polydisperse particles were sampled onto a quartz filter at a flow rate of 10 L min^{-1}. The filter was promptly extracted with 2 mL acetonitrile by sonicating for 12 min, followed by ESI-MS analysis. In type (i) experiments, SOA formed in the absence of formic acid was also impacted onto a germanium (Ge) attenuated total reflectance (ATR) crystal using a custom designed impactor[54] at a flow rate of 30 L min^{-1} for 10 min for ATR-Fourier transform infrared (ATR-FTIR) measurements.

In both the flow reactor and chamber experiments, a 10 cm monolith extruded carbon denuder (Novacarb™; Mast Carbon, Ltd) was inserted in front of the filter to remove the gas phase species before particle collection. Particle size distributions obtained with and without the denuder show no significant difference. Blank experiments were also performed with the same experimental procedures as the ozonolysis experiments except that O_3 was not added to the flow reactor or the chamber. Particle number concentrations were <10 cm^{-3} in blank experiments. No seed particles were added in any of these experiments.

SOA characterization

ESI-MS measurements. Acetonitrile extracts of both SOA samples and blanks were analyzed by ESI-MS. The ESI source was operated in positive ion mode under optimum conditions as follows: capillary voltage 3.0 kV, desolvation gas flow 500 L h^{-1}, and desolvation gas temperature 120 °C. Mass spectra were acquired over a mass range of 200–1000 Da. Ions observed were

primarily sodium adducts, $[M + Na]^+$. Mass spectra of blanks, which contained peaks attributable mainly to the impurities from the filter and acetonitrile solvent, were subtracted from the spectra of SOA samples. Data analysis was performed using MassLynx software. Accurate mass measurements were performed using polyethylene glycol, polyethylene glycol monomethyl ether, or sodium formate as the mass calibration standards.

AMS measurements. An Aerodyne HR-ToF-AMS was used to measure the chemical compositions of size-selected particles (50, 75, 100, 150, and 200 nm) in the flow reactor experiments. Details of this instrument have been described elsewhere.[58] Briefly, SOA particles sampled into the AMS (40–1000 nm) are focused into a particle beam using an aerodynamic lens. The particles travel through a size-selecting vacuum chamber and are then vaporized at 600 °C. The resulting vapors are ionized by electron impact (70 eV) and analyzed with a ToF mass analyzer. Elemental analysis was performed using the "Improved-Ambient" method.[59] Measurements of effective density were made as a function of particle diameter using the ratio of vacuum aerodynamic diameter to SMPS mobility diameter, assuming the particles are spherical.[60]

ATR-FTIR measurements. SOA particles from the chamber were impacted onto a Ge ATR crystal that was transferred immediately into an ATR cell (volume ~2 cm^3) through which dry synthetic air was flowed at 30 ml min^{-1}. A Nicolet 6700 FTIR spectrometer (Thermo Scientific) was used to record single beam spectra of the crystal before and after the SOA was deposited, at a resolution of 4 cm^{-1}. One hundred and twenty-eight scans were averaged for each spectrum. The absorbance spectra of SOA on the crystal were then obtained as $\log_{10}(S_0/S_1)$ where S_0 and S_1 represent a background and a spectrum of interest, respectively.

Results and discussion

Particle formation in the flow reactor with or without an OH scavenger

Fig. 1 shows the ESI mass spectra of SOA particles formed from the ozonolysis of *trans*-3-hexene in the absence and presence of cyclohexane or chlorocyclohexane for 24 s reaction time in the flow reactor. Ions corresponding to $[M + Na]^+$ are observed across a mass range of 200–800 Da. In the mass spectrum obtained without a scavenger (Fig. 1a), an obvious feature is the presence of an ion series starting at *m*/*z* 305 with mass differences of *m*/*z* 74, suggesting the formation of oligomers with a repeat unit that has the same mass as *trans*-3-hexene SCI (CH_3CH_2CHOO). As discussed below, the species corresponding to *m*/*z* 305 is an oligomer formed from a hexene alkyl peroxy radical and two SCI.

Table 1 shows the assignment of different oligomer series observed in the ESI mass spectra. In the absence of a scavenger, OH radicals formed by ozonolysis with a yield[61] of ~47%, will react in air with *trans*-3-hexene, producing primarily $CH_3CH_2CH(OH)CH(OO^{\bullet})CH_2CH_3$ (hereafter referred to as HE-RO_2, MW 133) as the main RO_2 radicals. As observed in Fig. 1a, the ion series is consistent with the oligomers formed from HE-RO_2 + *n*SCI + HO_2 where *n* represents the number of SCI chain units. Hereafter, this oligomer series is termed as OLI-A. Accurate mass determinations (Table 2) on selected OLI-A oligomers

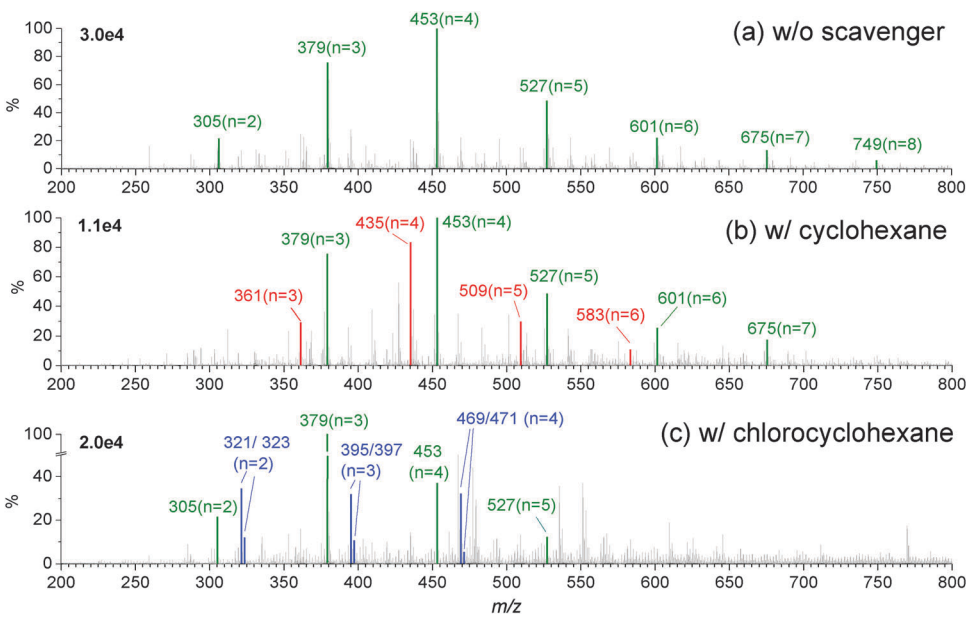

Fig. 1 Normalized ESI mass spectra of SOA from ozonolysis of *trans*-3-hexene in the flow reactor in the absence and presence of an OH scavenger. (a) Without scavenger; (b) with 6500 ppm cyclohexane; and (c) with 1800 ppm chlorocyclohexane. The initial concentrations of *trans*-3-hexene and O_3 are 12.5 ppm and 13 ppm, respectively. The peaks highlighted in green, red and blue correspond to three different oligomer series, *i.e.*, OLI-A, OLI-B, and OLI-C, respectively (see text). The values in the top-left corner of the spectra are the intensity of the peak to which other peaks are normalized. *n* represents the number of SCI chain units in oligomers.

Table 1 Summary of oligomer formation from the ozonolysis of *trans*-3-hexene in the flow reactor in the absence and presence of an OH scavenger

Scavenger	Oligomer series	Mechanisms	$n = 1^a$	$n = 2$	$n = 3$	$n = 4$	$n = 5$	$n = 6$	$n = 7$	$n = 8$
None	OLI-A	HE-RO_2 + SCI	$(231)^b$	305	379	453	527	601	675	749
Cyclohexane	OLI-B	CH-RO_2 + SCI	(213)	$(287)^b$	361	435	509	583		
Chlorocyclohexane	OLI-C	^{35}Cl-RO_2 + SCI	(247)	321	395	469				
		^{37}Cl-RO_2 + SCI	(249)	323	397	471				

[a] The values for the oligomer series correspond to the mass to charge (m/z) ratios of the $[M + Na]^+$ ions in the ESI-MS spectra; n represents the number of chain units in the oligomers. [b] These oligomers were not observed in the ESI-MS spectra probably because of their relatively higher volatility and thus lower contributions to the flow reactor SOA.

Table 2 Accurate mass data and elemental composition for different oligomer series formed in *trans*-3-hexene ozonolysis with and without OH or SCI scavengers

Oligomer series	No. of chain units	Observed accurate mass (Da)	Elemental composition	Calculated exact mass (Da)	Absolute mass error (mDa)	Relative mass error (ppm)
OLI-A	$n = 3$	379.1950	$C_{15}H_{32}O_9Na$	379.1944	0.6	1.6
	$n = 4$	453.2295	$C_{18}H_{38}O_{11}Na$	453.2312	−1.7	−3.7
	$n = 5$	527.2675	$C_{21}H_{44}O_{13}Na$	527.2680	−0.5	−0.9
OLI-B	$n = 3$	361.1821	$C_{15}H_{30}O_8Na$	361.1838	−1.7	−4.8
	$n = 4$	435.2189	$C_{18}H_{36}O_{10}Na$	435.2206	−1.7	−3.9
OLI-C	$n = 2$	321.1095	$C_{12}H_{23}O_6{}^{35}ClNa$	321.1081	1.4	4.4
	$n = 3$	395.1458	$C_{15}H_{29}O_8{}^{35}ClNa$	395.1449	0.9	2.4
OLI-D	$n = 1$	347.2057	$C_{15}H_{32}O_7Na$	347.2046	1.1	3.2
	$n = 2$	421.2400	$C_{18}H_{38}O_9Na$	421.2414	−1.4	−3.2

show very good agreement with their expected elemental compositions. The ESI-MS results presented here corroborate the oligomerization mechanism proposed by Sadezky and co-workers,[43] however our data show an increased contribution from longer oligomers, *i.e.*, $n > 5$, compared to the data reported by Sadezky *et al.*[43]

In the presence of an OH scavenger, the reaction between the scavenger and OH radicals contributes to the formation of a different RO_2 radical, which is also expected to initiate oligomerization, thus resulting in the formation of a different oligomer series. As shown in Fig. 1b and c, in addition to OLI-A, new oligomer series starting from m/z 361 or m/z 321 were observed in the presence of cyclohexane or chlorocyclohexane, respectively. These two new oligomer series (hereafter termed as OLI-B and OLI-C) are attributed to the reactions of CH-RO_2 + nSCI + HO_2 and Cl-RO_2 + nSCI + HO_2, where CH-RO_2 (MW 115) and Cl-RO_2 (MW 149) denote cyclohexyl peroxy and chlorocyclohexyl peroxy radicals produced by the reaction of OH with cyclohexane and chlorocyclohexane, respectively. Accurate mass measurements performed on selected m/z values were again in excellent agreement with the predicted elemental compositions of oligomers for each series, as reported in Table 2. As chlorine has two stable isotopes, ^{35}Cl and ^{37}Cl, OLI-C was detected as a series of doublet peaks with intensity ratios equal to that of the two isotopes, *i.e.*, 3 : 1.

In the presence of cyclohexane or chlorocyclohexane, >98% or >90%, respectively, of OH radicals should react with the scavenger based on the scavenger concentrations used relative to *trans*-3-hexene. The formation of CH-RO_2 and Cl-RO_2, therefore, would be expected to dominate over that of HE-RO_2. Accordingly, the gas phase formation of OLI-B and OLI-C should prevail over OLI-A. However, the OLI-A series is still significant in SOA particles formed in the presence of a scavenger as seen in the ESI mass spectra (Fig. 1b and c). This difference between gas phase formation and particle phase abundance of oligomers is likely due, at least in part, to the different volatilities of the oligomer series. For example, using the group-contribution method of Pankow and Asher,[36] the vapor pressures of oligomers n = 2, 3, 4, 5 in OLI-A at 295 K are estimated to be 1.5×10^{-9} atm, 3.2×10^{-11} atm, 6.8×10^{-13} atm, and 1.4×10^{-14} atm, respectively, over two orders of magnitude lower than those of oligomers n = 2, 3, 4, 5 in OLI-B, which are estimated to be 2.4×10^{-7} atm, 5.1×10^{-9} atm, 1.1×10^{-10} atm, and 2.3×10^{-12} atm at 295 K. Vapor pressures predicted using this method have an average uncertainty of a factor of two. However, such uncertainty would not alter the calculated relative vapor pressures of the oligomers. No values for halogenated subunits could be found in this group-contribution method. However, the vapor pressure of chlorocyclohexane has been reported to be 12 times lower than that of cyclohexane,[62,63] suggesting that OLI-C would be less volatile than OLI-B but still more volatile than OLI-A. These calculations suggest that although more OLI-B or OLI-C oligomers that incorporate CH-RO_2 or Cl-RO_2 are expected to be formed in the presence of an OH scavenger, their higher volatilities lead to smaller contributions to SOA. In addition, there may be steric hindrance to their formation because of the presence of the 6-membered rings in CH-RO_2 and Cl-RO_2 that could result in lower rate constants for CH-RO_2 + SCI and Cl-RO_2 + SCI. It is interesting to note that when chlorocyclohexane

is used, both the OLI-A and OLI-C series in Fig. 1c contain shorter oligomers than in the absence of the scavenger (Fig. 1a). This may be due to the consumption of SCI by some species (in addition to Cl-RO_2) formed uniquely in the presence of chlorocyclohexane, which suppresses the growth of the oligomer chain. It has been reported that the oxidation of chloroalkanes forms HCl,[64,65] and it is likely that HCl is also produced in the OH initiated oxidation of chlorocyclohexane. If HCl reacts with SCI, as discussed below, it will inhibit the formation of longer oligomers.

Particle formation in the chamber with or without SCI scavenger

Fig. 2 shows the ESI mass spectra of SOA particles formed from the ozonolysis of *trans*-3-hexene in the static chamber without or with formic acid as an SCI scavenger. Compared to flow reactor experiments where smaller particles were observed (mean size ~77 nm after a 24 s reaction), larger particles are measured in the chamber experiments (mean size ~135 nm after 18 min reaction time). The ESI mass spectrum in the absence of formic acid (Fig. 2a) is very similar to that obtained from the flow reactor without OH scavenger (Fig. 1a), except for a shift in relative intensity of the oligomers. The ESI mass spectra show that these chamber SOA particles at 18 min have a higher contribution from oligomers $n \leq 3$ than the flow reactor SOA particles at 24 s. This suggests a size-dependent growth mechanism for SOA particles. As discussed later, it appears that oligomers $n \geq 4$ play a more important role in the initial stages of particle formation, whereas oligomers $n \leq 3$ contribute mainly to particle growth. It can be seen in Fig. 2b and c that the presence of formic acid, which reacts with SCI,[5,45,66–68] strongly suppresses the formation of longer oligomers, confirming that SCI play a key role in oligomer formation.

It is worthwhile noting that there are two new peaks at *m*/*z* 347 and 421 in the mass spectra with 6 ppm formic acid, which are attributed to products from acid-catalyzed reactions in the particle phase. In order to verify this, we investigated SOA formation from ozonolysis of *trans*-3-hexene in the presence of gaseous hydrochloric acid (HCl). Fig. 3 shows the ESI mass spectra of SOA particles from ozonolysis of *trans*-3-hexene at different HCl concentrations. Similar to the addition of formic acid (Fig. 2), the presence of HCl significantly inhibits the formation of longer oligomers, suggesting that HCl can act as an SCI scavenger. Notably, at higher HCl concentrations, a new oligomer series starting at *m*/*z* 347 again with mass differences of 74 Da is formed in SOA. Hereafter, this oligomer series is termed as OLI-D. Considering that the mass of OLI-D is 116 Da higher relative to OLI-A and that this mass difference is the same as the molecular weight of the primary OH oxidation product of *trans*-3-hexene, $CH_3CH_2CH(OH)C(O)CH_2CH_3$ (hereafter referred to as HECAB), the OLI-D may be either product A (in reaction (R3a)) or product B (in reaction (R3b)) formed by the acid-catalyzed reaction of OLI-A with HECAB on the surface and/or in the bulk of SOA particles (product A or B in reaction (R3) would both be observed as $[M + Na]^+$ at *m*/*z* 347 in the mass spectra). Theoretical calculations have shown that the formation of product B in the particle phase is not thermodynamically favorable.[21] OLI-D, therefore, is more likely the peroxyhemiacetal product A. Accurate mass measurements (Table 2) of selected OLI-D oligomers agree well with the expected elemental composition for these peroxyhemiacetals. Formation of peroxyhemiacetals has also been suggested in SOA from ozonolysis of 1-tetradecene,[69] α-pinene,[16,23] and ethylene,[44] and photooxidation of dodecane[70] and toluene.[71]

Fig. 4 shows the number and mass concentrations, as well as the mean diameter of SOA particles formed from ozonolysis

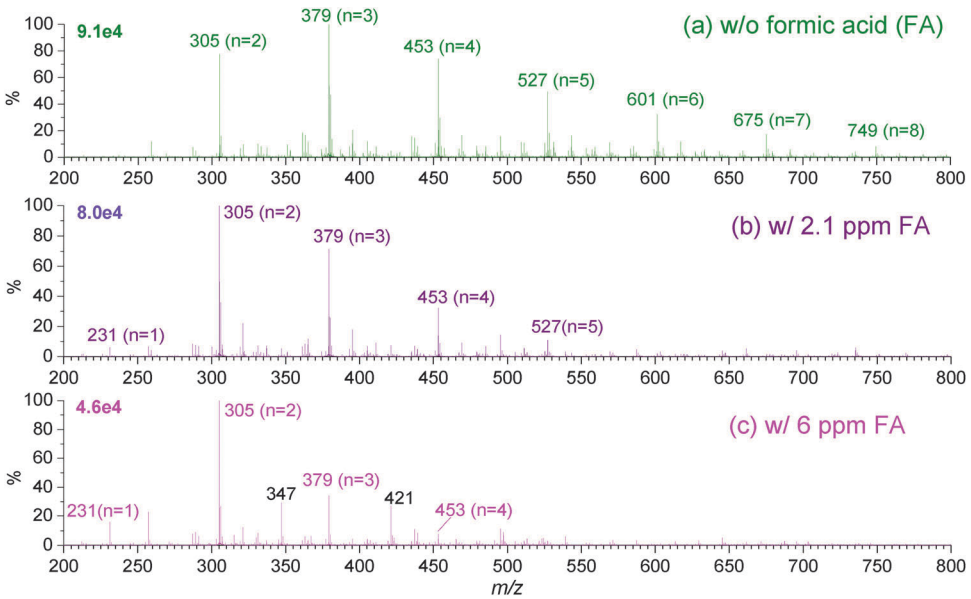

Fig. 2 Normalized ESI mass spectra of SOA particles from ozonolysis of *trans*-3-hexene in the static chamber for 18 min in the absence and presence of formic acid. (a) Without formic acid; (b) with 2.1 ppm formic acid; and (c) with 6 ppm formic acid. The initial concentrations of *trans*-3-hexene and O_3 are 10 ppm each. The values in the top-left corner of the spectra are the intensity of the peak to which other peaks are normalized. *n* represents the number of SCI chain units in oligomers.

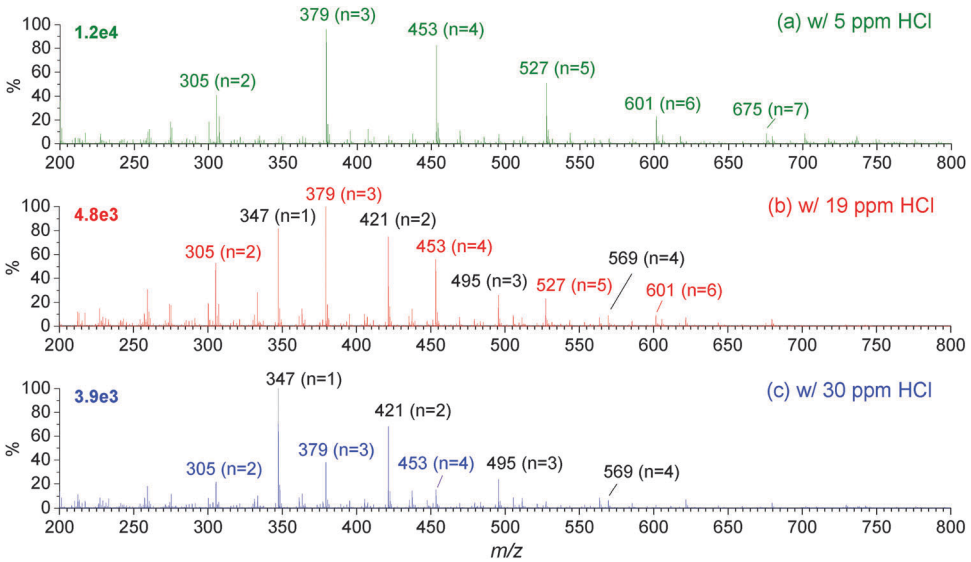

Fig. 3 Normalized ESI mass spectra of SOA particles from ozonolysis of *trans*-3-hexene in the static chamber for 18 min in the presence of (a) 5 ppm, (b) 19 ppm, and (c) 30 ppm HCl. The initial concentrations of *trans*-3-hexene and O_3 are 10 ppm each. The values in the top-left corner of the spectra are the intensity of the peak to which other peaks are normalized. *n* represents the number of SCI chain units in oligomers.

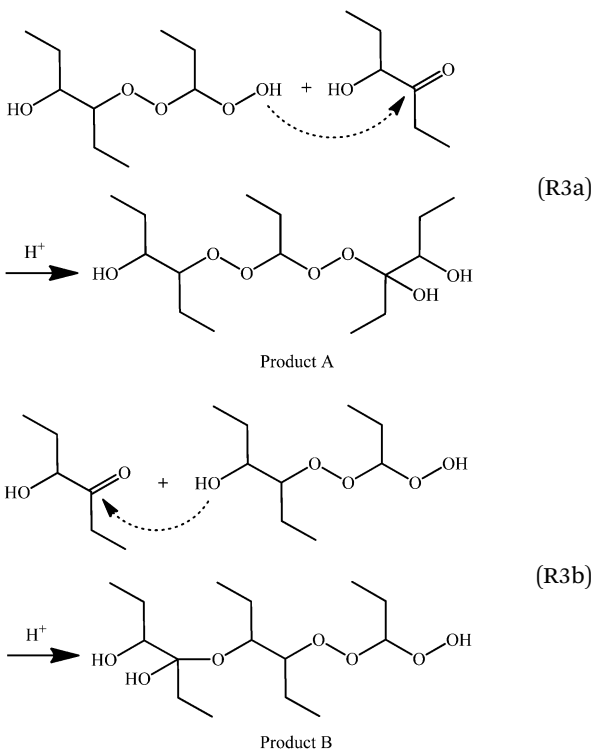

(R3a)

(R3b)

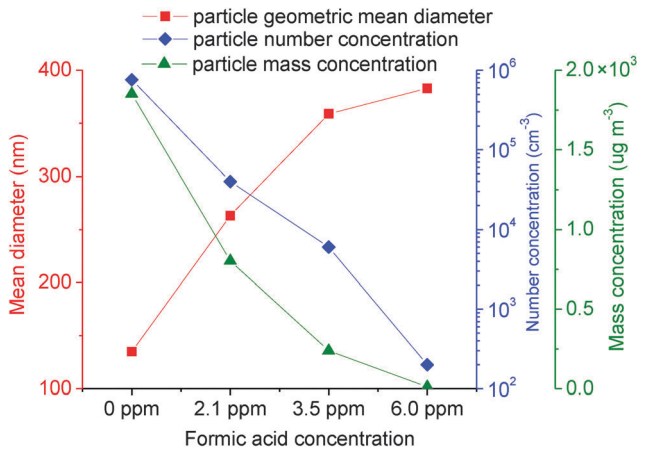

Fig. 4 Mean diameter, number and mass concentration of SOA particles from ozonolysis of *trans*-3-hexene in the chamber at different formic acid concentrations. The initial concentrations of *trans*-3-hexene and O_3 are 10 ppm each. Reaction time is 18 min. An average density of 0.9 g cm^{-3} was used to calculate mass concentration of *trans*-3-hexene SOA (see Fig. 8b).

of *trans*-3-hexene at different formic acid concentrations. In addition to suppressing formation of longer oligomers, the presence of formic acid also significantly inhibited new particle formation while enhancing particle growth. This was also observed in experiments with HCl. These results suggest that long oligomers are the key nucleating species for particle formation, while condensable species (*e.g.*, short oligomers) are still being formed that can contribute to particle growth. Given the smaller number of particles that occur in the presence of formic acid, there should be more low MW condensable species available in the gas phase for each particle to grow to larger sizes.

Recently, Sakamoto *et al.*[44] observed the gas phase formation of oligomers containing SCI as the chain unit during ethylene ozonolysis and proposed a new oligomer formation mechanism (reaction (R2)) involving sequential addition of SCI to organic hydroperoxides (ROOHs) instead of to RO_2 radicals. The hydroperoxides included 2-hydroxylethyl hydroperoxide ($HOCH_2CH_2OOH$) produced by OH oxidation of ethylene, and formyloxymethyl hydroperoxide ($HCOOCH_2OOH$) formed from reaction of formic acid with SCI.

To test the contribution of this mechanism in the current system, oligomer formation from ozonolysis of *trans*-3-hexene

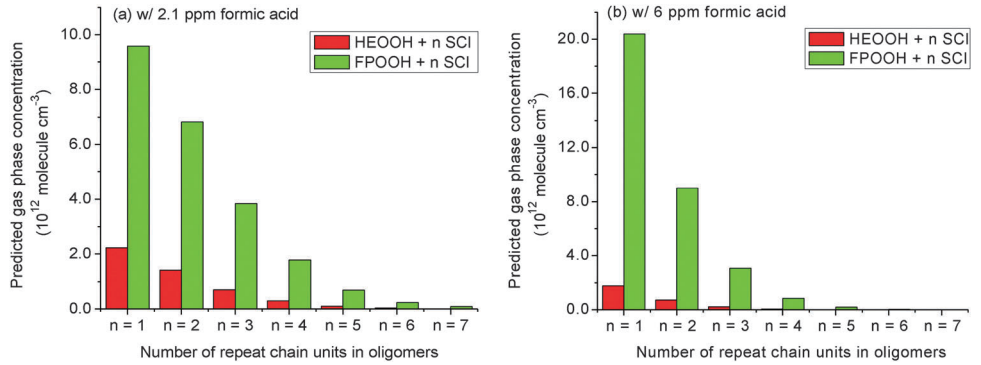

Fig. 5 Box model predicted gas phase oligomer concentration from ozonolysis of *trans*-3-hexene in the presence of (a) 2.1 ppm and (b) 6 ppm formic acid. No partitioning into particles is assumed. In the model, the initial concentrations of *trans*-3-hexene and O_3 are 10 ppm each, and reaction time is 10 min. Oligomers are assumed to be produced by HEOOH + *n*SCI and FPOOH + *n*SCI, where HEOOH and FPOOH denote organic hydroperoxides from HE-RO_2 + HO_2 and formic acid + SCI reactions, respectively. The rate constants of both oligomer formation pathways are assumed to be 5×10^{-12} cm^3 $molecule^{-1}$ s^{-1}.

in the presence of formic acid was simulated using a box model by assuming that oligomers are formed through ROOH + *n*SCI (see details in the ESI†).

Fig. 5 shows the model-predicted gas phase formation of oligomers through sequential addition of SCI to the two dominant organic hydroperoxides formed during the ozonolysis, *i.e.*, *trans*-3-hexene derived hydroperoxide (HEOOH) from HE-RO_2 + HO_2 reaction and 1-formyloxypropyl hydroperoxide (FPOOH) from formic acid + SCI reaction. The predicted concentrations of oligomers from FPOOH + *n*SCI are about 5 and 10 times higher than those from HEOOH + *n*SCI in the presence of 2.1 and 6 ppm formic acid, respectively. Using a group-contribution method,[36] the vapor pressures of oligomers n = 2, 3, 4 of FPOOH + *n*SCI are estimated to be 1.2×10^{-7} atm, 2.5×10^{-9} atm, and 5.3×10^{-11} atm, respectively, while the oligomers n = 2, 3, 4 of HEOOH + *n*SCI are approximately 1.5×10^{-9} atm, 3.2×10^{-11} atm, and 6.8×10^{-13} atm. Although the vapor pressure of FPOOH + *n*SCI is about two orders of magnitude higher than HEOOH + *n*SCI, it is comparable to that of HEOOH + $(n-1)$SCI. Given that the predicted gas phase concentration of oligomers from FPOOH + *n*SCI is substantially higher than that for HEOOH + $(n-1)$SCI (Fig. 5), the former oligomer series should have a greater contribution to SOA formation than the latter. However, the ESI-MS spectra of *trans*-3-hexene SOA in Fig. 2 show no evidence of oligomers from FPOOH + *n*SCI, *e.g.*, no obvious peaks at *m*/*z* 291 (n = 2), 365 (n = 3), and 439 (n = 4). This suggests that oligomers observed in the present study are not formed by ROOH + *n*SCI, but rather by RO_2 + *n*SCI.

Particle formation at lower concentrations and different relative humidities

The reaction of SCI with water vapor is considered an important, sometimes dominant, loss pathway for SCI in the atmosphere, with the extent depending on the types of SCI.[45,67,68,72–74] In order to evaluate the influence of water vapor on both oligomer and new particle formation from ozonolysis, we conducted chamber experiments over a wide range of relative humidities using 800 ppb *trans*-3-hexene and 1.5 ppm O_3.

Fig. 6 shows the ESI mass spectra of SOA particles formed from ozonolysis of 800 ppb *trans*-3-hexene at different RH. SOA particles formed at 800 ppb (Fig. 6a) have a greater contribution from shorter oligomers compared to those formed at higher concentrations (Fig. 2a). As the formation of SCI based oligomers involves multistep reactions, higher reactant concentrations favor the formation of longer oligomers. As observed in Fig. 6b and c, under humid conditions, the presence of water significantly inhibits the formation of long oligomers ($n \geq 4$) by scavenging SCI, but the formation of short oligomers is still evident even at 80% RH. Interestingly, the peroxyhemiacetals (at *m*/*z* 347 and 421) observed in the acid-catalyzed particle phase reaction of OLI-A with HECAB discussed above, are also formed in SOA with their abundance increasing with rising RH. It has been reported that under humid conditions Criegee intermediates can react with water to form acids[73–76] and/or hydroxyhydroperoxides (HHPs).[76–79] HHPs can subsequently decompose to either aldehydes/ketones and H_2O_2 or acids and H_2O,[77,78,80] with the decomposition being assisted by the presence of water vapor.[79,80] Therefore, as RH increases more acids will be produced,[75,76,78] thus favoring the formation of peroxyhemiacetals.

Fig. 7 illustrates particle formation from ozonolysis as a function of RH. Despite the suppressed production of key nucleating species (*i.e.*, oligomers $n \geq 4$), particle number concentration increases unexpectedly with increasing RH. Considering the reaction products derived from *trans*-3-hexene SCI and H_2O (*e.g.*, 1-hydroxypropyl hydroperoxide, HPOOH) are too volatile to act as nucleating species, water may be involved in growing small clusters to detectable sizes. For example, clusters from oligomeric products could H-bond to water *via* the –OH, O–O and –OOH groups in the oligomer. Once a substantial number of new particles are formed, they cannot grow to large sizes because of the lack of adequate condensable material.

Size-dependent composition and density of SOA

As discussed above, the longer oligomers ($n \geq 4$) appear to be the key nucleating species for particle formation, while the

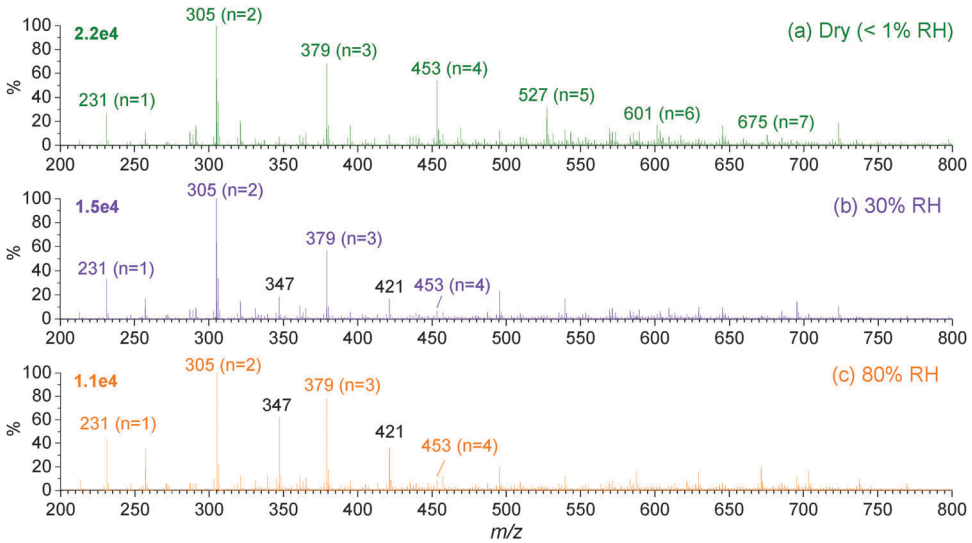

Fig. 6 Normalized ESI mass spectra of SOA particles from ozonolysis of *trans*-3-hexene in the chamber at lower concentrations and different relative humidities. The initial concentrations of *trans*-3-hexene and O_3 are 800 ppb and 1.5 ppm, respectively. Reaction time is 20 min. The values in the top-left corner of the spectra are the intensity of the peak to which other peaks are normalized. *n* represents the number of SCI chain units in oligomers.

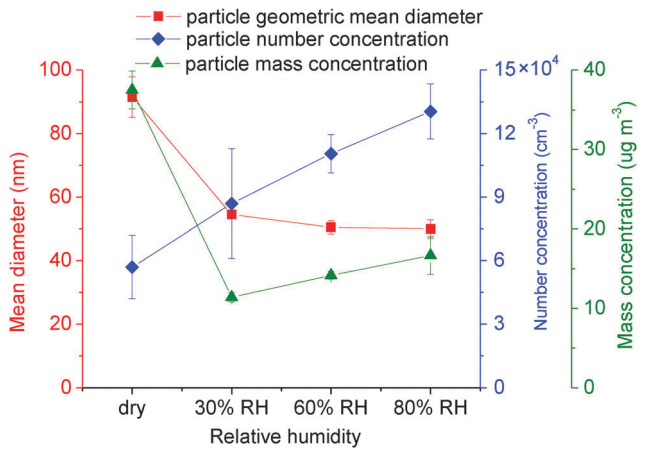

Fig. 7 Mean diameter, number and mass concentration of SOA particles from ozonolysis of *trans*-3-hexene in the chamber at different relative humidities. The initial concentrations of *trans*-3-hexene and O_3 are 800 ppb and 1.5 ppm, respectively. Reaction time is 20 min. An average density of 0.9 g cm^{-3} was used to calculate mass concentration of SOA (see Fig. 8b).

shorter oligomers mainly contribute to particle growth. To test this hypothesis we conducted chemical composition measurements of size-selected SOA particles formed in the flow reactor using ESI-MS and HR-ToF-AMS. The results are shown in Fig. 8. The oligomer peaks in the ESI mass spectra of size-selected particles were separated into three groups, *i.e.*, $n = 3$, $n = 4$–5, and $n = 6$–8 according to the MW of the oligomers. Because the $n = 2$ peak in the mass spectra has very low intensity and there is an interfering peak in the blanks, it was not included in the analysis. Fig. 8a shows the fraction of oligomer intensity in each group to the total oligomer intensity, for the particles of different sizes (80, 150 and 210 nm). Higher order oligomers ($n \geq 4$) comprise a greater fraction of the total for smaller particles, while shorter oligomers ($n = 3$) contribute relatively more to the larger particles.

AMS measurements provide complementary information to the ESI-MS data. The harsh analysis conditions (vaporization at 600 °C and electron impact ionization at 70 eV) in AMS lead to significant fragmentation of organic species. However, high MW fragments (>150 Da) are still observed in AMS spectra of size-selected particles. Fig. 8b shows the fraction of the total intensity for >150 Da fragments in the mass spectra as a function of the particle size from 50–200 nm. The fraction of high MW fragments decreases significantly with increasing particle size, indicating that smaller particles contain substantially more high MW compounds, *i.e.*, oligomers. (It is noted that larger, multiply charged particles can also contribute to these size-selected samples with more highly charged particles mimicking smaller ones; this would lead to an underestimate of the observed trend.) Fig. 8b also shows the effective density of SOA as a function of particle size. The density decreases from 1.12 g cm^{-3} for 50 nm particles to 0.82 g cm^{-3} for 200 nm particles. Such a density gradient implies a change in composition as the particle grows.

Fig. 8c shows size-dependent O/C and H/C ratios of the particles, obtained by AMS. As the particles grow to larger sizes, the O/C ratio decreases from 0.57 ± 0.09 for 75 nm particles to 0.46 ± 0.02 for 200 nm particles. Correspondingly, the H/C ratio increases from 1.90 ± 0.16 to 2.09 ± 0.02. The O/C ratio of the smallest measured particles (75 nm) is within experimental error of that of the observed oligomers (*e.g.*, for $n = 4$, O/C = 0.61). This suggests that the growth of particles is due to uptake of less oxygenated species (Again, the presence of larger, multiply charged particles may lead to an underestimate in O/C ratios). A similar negative correlation between the O/C ratio and particle size has also been shown for α-pinene/O_3 SOA generated in a flow reactor by Tolocka *et al.*[12] It is worth noting that

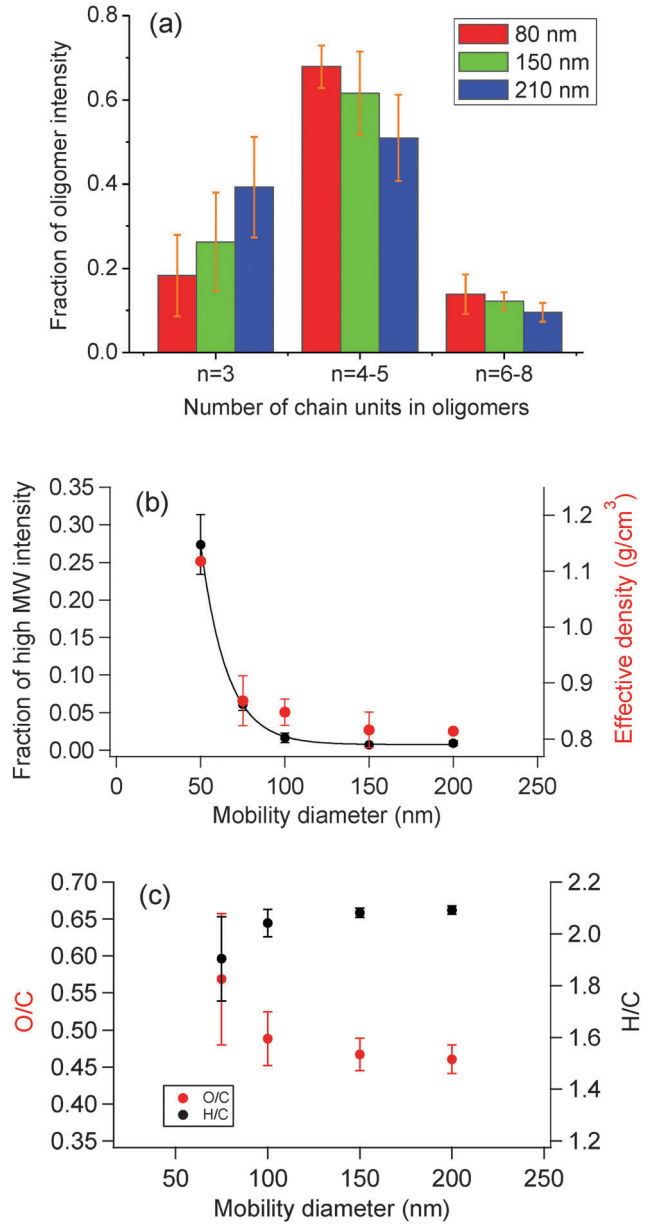

Fig. 8 Size-dependent composition of SOA particles formed from ozonolysis of *trans*-3-hexene in the flow reactor. (a) Intensity fraction of oligomers measured by ESI-MS; *n* represents the number of SCI chain units in the oligomer. (b) Intensity fraction of high molecular weight fragments (>150 amu) detected by AMS (left *y*-axis, black); effective density of *trans*-3-hexene SOA (right *y*-axis, red). (c) O/C and H/C ratios obtained by AMS; The O/C and H/C ratios of 50 nm particles were not included because of their very low mass loading which results in a high uncertainty in the elemental ratio analysis. The error bars are the largest for the smallest particles because of the low mass loading. However, the data from several experiments show a clear trend of decreasing O/C and increasing H/C as a function of diameter, with good precision within each experiment.

the substantial decrease in density as a function of particle size is well correlated with the decrease in the O/C ratio. This is consistent with previous measurements of the density of organic aerosol, which showed that more oxidized particles have higher density.[81,82]

The size-dependent data support the hypothesis that SOA particles from ozonolysis of *trans*-3-hexene are initially formed by nucleation of higher molecular weight oligomers ($n \geq 4$) and then grow *via* condensation of shorter oligomers and other less oxygenated, more volatile species.[12,30,31,38,39]

Phase state of SOA

The phase of atmospheric particles (liquid/solid) plays a crucial role in various physical and chemical processes of particles such as growth,[49,50,52] aging,[47,48,52,53] and water uptake.[48,51] In the present study, particle impaction/ATR-FTIR measurements were performed to offer some insight into the phase/viscosity of *trans*-3-hexene SOA since the impaction patterns on the Ge crystal have been shown to be an indicator of phase.[54] For example, viscous liquid particles hit and stick to the crystal to form a row of spots, whereas solid particles above a certain size bounce and can be subsequently captured on the crystal, forming a disperse pattern dubbed "clouds".[54] Fig. 9 shows a photograph of a typical impaction pattern of *trans*-3-hexene SOA on a Ge ATR crystal. For comparison, the impaction pattern of SOA formed from α-pinene ozonolysis obtained in a previous study[54] in our lab using the same impactor is also shown. The *trans*-3-hexene SOA flows away from the centerline that is the initial area of impact on the ATR crystal. This is in contrast to the behavior of semi-solid α-pinene SOA which bounces but is subsequently captured on the crystal, forming a more diffuse "cloud" pattern. The lack of "bounce" establishes that *trans*-3-hexene SOA is less viscous than α-pinene SOA.

Fig. 10a shows a typical ATR-FTIR spectrum of *trans*-3-hexene SOA collected immediately following impaction. An obvious feature of the spectrum is the presence of strong bands between 800–1200 cm^{-1}, likely because of the O–O and C–O stretching vibrations in the C–O–O group.[83] The band attributable to C=O at ~1738 cm^{-1} is weaker. This is consistent with the ESI-MS data, which suggest *trans*-3-hexene SOA is mainly comprised of oligomers in which the repeat chain unit contains a C–O–O group. Fig. 10b is a difference spectrum showing the changes in SOA upon exposure to a flow of clean dry air (30 mL min^{-1}) for 20 hours. More volatile organic species in SOA

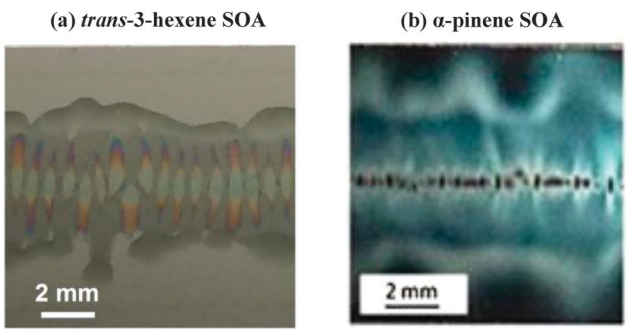

Fig. 9 Digital photography of the impaction pattern of (a) *trans*-3-hexene and (b) α-pinene SOA on the ATR crystal. The impaction pattern of α-pinene SOA acquired in a previous study[54] using the same impactor is displayed for comparison. The photographs are of a 1 × 1 cm section of the ATR crystal.

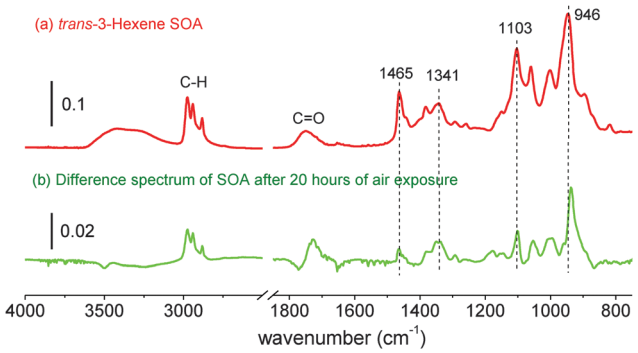

Fig. 10 (a) A typical ATR-FTIR spectrum of SOA from ozonolysis of *trans*-3-hexene. This spectrum is derived from $\log_{10}(S_0/S_1)$ where S_0 is the single beam spectrum of the clean crystal and S_1 is that of SOA covered crystal recorded immediately following impaction. (b) A typical difference spectrum of SOA upon exposure to a flow of clean dry air for 20 hours. This spectrum is $\log_{10}(S_1/S_{20})$ where S_1 is the single beam spectrum of SOA covered crystal immediately following impaction and S_{20} is that after 20 hours of air exposure. The positive peaks in the spectrum represent an apparent increase in the functional groups over the 20 h (see text).

may evaporate under such circumstances, leading to a decrease in the peak intensities associated with those species. The ESI mass spectra of SOA extracted from the crystal immediately following impaction and after 20 hours of air exposure showed that there is a preferential loss of oligomer $n = 1$ ($\sim$100%) and $n = 2$ ($\sim$65%) relative to $n \geq 3$ from the SOA on exposure to air. However, as can be seen in Fig. 10b, the absorbance of many SOA peaks actually increases. This is attributed to the spreading of SOA across the crystal under the air flow. The depth of penetration of the IR beam at 1750 and 2950 cm^{-1} for SOA with a refractive index of $\sim$1.5[84,85] on a Ge crystal is calculated to be 0.38 and 0.23 μm respectively.[86] If the initial film thickness along and close to the centerline is much larger than this, only a portion of the SOA is probed. As the film spreads out on the crystal, more of the SOA is probed by the IR beam, leading to the increase in absorbance. This supports the conclusion that *trans*-3-hexene SOA is less viscous than α-pinene SOA. In the latter case negative peaks were observed in the difference spectrum.[38]

Comparison to particle formation from α-cedrene

Our study, together with earlier work by Sadezky *et al.*[43] suggests that formation of oligomers involving RO_2 + *n*SCI is a major contributor to SOA formation during the ozonolysis of small alkenes. Given that substitution normally has significant effects on the reactivity and chemistry of SCI,[10,45,67,68] the mechanism of particle formation from the ozonolysis may vary with the molecular size and structure of the precursor alkenes. This poses the question as to how prevalent the RO_2 + *n*SCI mechanism is in oligomer and SOA formation from ozonolysis of large and complex alkenes such as terpenes and sesquiterpenes. In order to get some insight into this question, we carried out flow reactor ozonolysis experiments with α-cedrene, a sesquiterpene structurally similar to α-pinene, in the absence and presence of cyclohexane. When the latter was present, it was at a sufficiently high concentration to react with >98% of OH radicals produced during ozonolysis.

Fig. 11 shows typical ESI-MS spectra of SOA particles formed from ozonolysis of α-cedrene in the absence and presence of cyclohexane. Formation of α-cedrene derived monomers (*m*/*z* 240–350) and oligomers (*m*/*z* > 420) is evident both with and without cyclohexane. In the presence of cyclohexane, two additional oligomer patterns at *m*/*z* 350–410 and *m*/*z* 620–680 are formed in the SOA, likely resulting from the combination of the oxidation products of cyclohexane and α-cedrene. However, there are only minor contributions from peaks at *m*/*z* 391, 643, and 895, which would correspond to the potential oligomeric products from sequential addition of α-cedrene SCI to cyclohexane derived RO_2 ($CH\text{-}RO_2$) radicals. This is despite the high yield (>88%) of α-cedrene SCI from ozonolysis.[87] Thus,

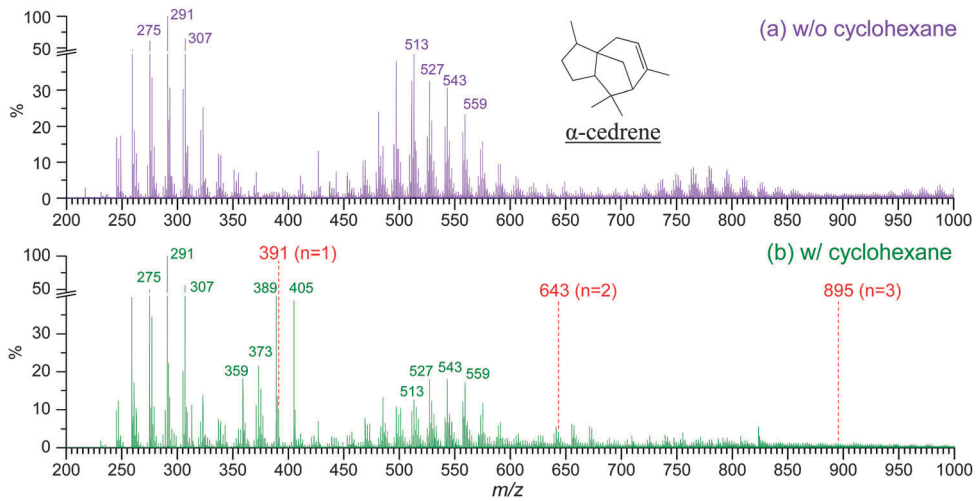

Fig. 11 Normalized ESI-MS spectra of SOA from the ozonolysis of α-cedrene in the (a) absence and (b) presence of cyclohexane in the flow reactor. The initial concentrations of α-cedrene, O_3, and cyclohexane are 500 ppb, 16 ppm, and 262 ppm, respectively. The reaction time is 30 s. Red dashed lines provide a visual guide to the position of the peaks expected for the potential oligomeric products from reaction of α-cedrene SCI with cyclohexane derived RO_2 radicals (RO_2 + *n*SCI).

the RO_2 + *n*SCI mechanism that dominates in the *trans*-3-hexene ozonolysis seems not to be prevalent in SOA formation from α-cedrene oxidation. One potential reason is that α-cedrene SCI may have a very low reactivity towards RO_2 radicals because of steric effects attributable to the structure of this SCI. As a result, other reactions may be more important in particle formation.[87,88] For example, it has been suggested recently that highly oxidized ELVOC formed by ozonolysis of α-pinene play a critical role in the nucleation and growth of SOA particles.[29,30,32,35] Given that α-cedrene is similar to α-pinene in structure, α-cedrene ozonolysis may also be able to produce such ELVOC.

Recently, Yao and coworkers have shown that during the ozonolysis of α-cedrene, the addition of an SCI scavenger, acetic acid, led to fewer particles but higher SOA mass yield.[87] Similar SCI scavenger effects have been observed for ozonolysis of β-pinene[20] and β-caryophyllene[89] in the presence of formic acid. In contrast, in the present study with *trans*-3-hexene, while the presence of formic acid inhibits new particle formation, it also strongly decreases SOA mass loading (Fig. 4). One explanation for this difference is that the products of reactions between large terpene SCI and the scavenger have low enough volatility to contribute significantly to particle growth, leading to a high SOA mass,[20,87,89] whereas the 1-formyloxypropyl hydroperoxide (FPOOH), produced by the reaction of small *trans*-3-hexene SCI with formic acid, is too volatile (the vapor pressure is estimated to be 2.6×10^{-4} atm at 295 K using a group-contribution method)[36] to significantly contribute to particle growth.

Conclusions and atmospheric implications

These studies show that particle formation in the *trans*-3-hexene ozonolysis is consistent with the sequential addition of SCI to RO_2 radicals as previously proposed by Sadezky *et al.*[43] Size-dependent oligomeric and elemental composition of SOA particles show that longer oligomers play a key role in initial particle formation and that subsequent growth occurs by condensation of shorter oligomers and other less oxygenated, more volatile products. In addition, impaction/ATR-FTIR measurements show that *trans*-3-hexene SOA is less viscous than α-pinene SOA.

However, the results of the α-cedrene ozonolysis experiments suggest that such oligomerization reactions may not play a major role in particle formation from large alkenes such as terpenes and sesquiterpenes. In these cases, it may be that the recently proposed ELVOC formation involving a series of intramolecular H abstractions/O_2 additions *via* RO_2 radicals[30,32,34] from ozonolysis is the major particle formation pathway.[30] Compared to terpene-RO_2 (*e.g.*, from α-pinene) where the structure favors the intramolecular H abstractions to produce ELVOC, the RO_2 radicals produced during ozonolysis of small alkenes may be too short to go through that pathway.

Considering that small alkenes make up a substantial fraction of VOCs in the atmosphere,[90,91] oligomer formation involving addition of their SCI to RO_2 radicals can have implications for atmospheric particle formation. However, in the atmosphere, such oligomer formation is expected to be strongly influenced by other gas phase species that can competitively react with RO_2 and SCI. For example, RO_2 radicals can also react with NO, HO_2, and other RO_2 in the atmosphere, with the relative importance depending particularly on the NO concentration.[5,45,92] Vereecken *et al.*[45] suggested that in a tropical forest area (*e.g.*, Suriname) the RO_2 + SCI reactions accounted for only 0.1% of RO_2 losses, assuming a rate constant of 5×10^{-12} cm^3 $molecules^{-1}$ s^{-1}. However, they point out that this rate constant was a conservative estimate and it could be on the order of 10^{-11} cm^3 $molecules^{-1}$ s^{-1}. In addition, SCI react with a number of other atmospheric species, *e.g.*, H_2O, SO_2, NO_2, carboxylic acids, as well as carbonyl and hydroxyl compounds.[5,45,66–68,72,93–95] Bimolecular reactions with these scavengers, in particular H_2O, have been suggested to be the dominant loss pathway of some SCIs in the atmosphere.[45,67,72] However, in the present study, water vapor was shown to increase new particle formation while decreasing the total mass.

Although the RO_2 + SCI reactions may not be important as a major loss process for RO_2 and SCI in the atmosphere, these reactions produce high molecular weight highly oxidized oligomeric products that have sufficiently low volatilities to form SOA. Moreover, in some circumstances scavenging of SCI may not necessarily suppress particle formation. For example, in the presence of SO_2, the reactions between SCI and SO_2 can lead to the formation of H_2SO_4,[5,74,93,96,97] an important nucleation precursor.[98,99]

A quantitative evaluation of the atmospheric importance of RO_2 + SCI reactions is not possible at the moment because of the large uncertainties in the rate constants for bimolecular reactions of SCI,[45,67] especially those of RO_2 + SCI reactions for which experimental data are not available. Therefore, further studies of the bimolecular chemistry of SCI are needed in order to better understand the RO_2 + SCI chemistry and its impacts on SOA formation in the atmosphere.

Acknowledgements

The authors gratefully thank National Science Foundation (Grants # 0909227 and 1207112) for support of this work, and the NSF Major Research Instrumentation (MRI) program (Grant # 0923323 and 1337080) for HR-ToF-AMS.

References

1 M. Hallquist, J. C. Wenger, U. Baltensperger, Y. Rudich, D. Simpson, M. Claeys, J. Dommen, N. M. Donahue, C. George, A. H. Goldstein, J. F. Hamilton, H. Herrmann, T. Hoffmann, Y. Iinuma, M. Jang, M. E. Jenkin, J. L. Jimenez, A. Kiendler-Scharr, W. Maenhaut, G. McFiggans, T. F. Mentel, A. Monod, A. S. H. Prevot, J. H. Seinfeld, J. D. Surratt, R. Szmigielski and J. Wildt, *Atmos. Chem. Phys.*, 2009, **9**, 5155–5236.

2 J. L. Jimenez, M. R. Canagaratna, N. M. Donahue, A. S. H. Prevot, Q. Zhang, J. H. Kroll, P. F. DeCarlo, J. D. Allan, H. Coe, N. L. Ng, A. C. Aiken, K. S. Docherty, I. M. Ulbrich, A. P. Grieshop, A. L. Robinson, J. Duplissy, J. D. Smith, K. R. Wilson, V. A. Lanz, C. Hueglin, Y. L. Sun, J. Tian, A. Laaksonen, T. Raatikainen, J. Rautiainen, P. Vaattovaara, M. Ehn, M. Kulmala, J. M. Tomlinson, D. R. Collins, M. J. Cubison, E. J. Dunlea, J. A. Huffman, T. B. Onasch, M. R. Alfarra, P. I. Williams, K. Bower, Y. Kondo, J. Schneider, F. Drewnick, S. Borrmann, S. Weimer, K. Demerjian, D. Salcedo, L. Cottrell, R. Griffin, A. Takami, T. Miyoshi, S. Hatakeyama, A. Shimono, J. Y. Sun, Y. M. Zhang, K. Dzepina, J. R. Kimmel, D. Sueper, J. T. Jayne, S. C. Herndon, A. M. Trimborn, L. R. Williams, E. C. Wood, A. M. Middlebrook, C. E. Kolb, U. Baltensperger and D. R. Worsnop, *Science*, 2009, **326**, 1525–1529.

3 M. Kanakidou, J. H. Seinfeld, S. N. Pandis, I. Barnes, F. J. Dentener, M. C. Facchini, R. Van Dingenen, B. Ervens, A. Nenes, C. J. Nielsen, E. Swietlicki, J. P. Putaud, Y. Balkanski, S. Fuzzi, J. Horth, G. K. Moortgat, R. Winterhalter, C. E. L. Myhre, K. Tsigaridis, E. Vignati, E. G. Stephanou and J. Wilson, *Atmos. Chem. Phys.*, 2005, **5**, 1053–1123.

4 N. L. Ng, M. R. Canagaratna, Q. Zhang, J. L. Jimenez, J. Tian, I. M. Ulbrich, J. H. Kroll, K. S. Docherty, P. S. Chhabra, R. Bahreini, S. M. Murphy, J. H. Seinfeld, L. Hildebrandt, N. M. Donahue, P. F. DeCarlo, V. A. Lanz, A. S. H. Prevot, E. Dinar, Y. Rudich and D. R. Worsnop, *Atmos. Chem. Phys.*, 2010, **10**, 4625–4641.

5 B. J. Finlayson-Pitts and J. N. Pitts, *Chemistry of the upper and lower atmosphere: theory, experiments, and applications*, Academic Press, San Diego, 2000.

6 J. H. Seinfeld and S. N. Pandis, *Atmospheric Chemistry and Physics: From Air Pollution to Climate Change*, J. Wiley, Hoboken, NJ, 2006.

7 J. H. Kroll and J. H. Seinfeld, *Atmos. Environ.*, 2008, **42**, 3593–3624.

8 P. J. Ziemann and R. Atkinson, *Chem. Soc. Rev.*, 2012, **41**, 6582–6605.

9 IPCC, Summary for Policymakers, in *Climate Change 2013: The Physical Science Basis. Contribution of Working Group I to the Fifth Assessment Report of the Intergovernmental Panel on Climate Change*, ed. T. F. Stocker, D. Qin, G. -K. Plattner, M. Tignor, S. K. Allen, J. Boschung, A. Nauels, Y. Xia, V. Bex and P. M. Midgley, Cambridge University Press, Cambridge, United Kingdom and New York, NY, USA, 2013.

10 D. Johnson and G. Marston, *Chem. Soc. Rev.*, 2008, **37**, 699–716.

11 A. Lee, A. H. Goldstein, M. D. Keywood, S. Gao, V. Varutbangkul, R. Bahreini, N. L. Ng, R. C. Flagan and J. H. Seinfeld, *J. Geophys. Res.*, 2006, **111**, DOI: 10.1029/2005JD006437.

12 M. P. Tolocka, K. J. Heaton, M. A. Dreyfus, S. Y. Wang, C. A. Zordan, T. D. Saul and M. V. Johnston, *Environ. Sci. Technol.*, 2006, **40**, 1843–1848.

13 M. P. Tolocka, M. Jang, J. M. Ginter, F. J. Cox, R. M. Kamens and M. V. Johnston, *Environ. Sci. Technol.*, 2004, **38**, 1428–1434.

14 W. A. Hall and M. V. Johnston, *Aerosol Sci. Technol.*, 2011, **45**, 37–45.

15 K. J. Heaton, M. A. Dreyfus, S. Wang and M. V. Johnston, *Environ. Sci. Technol.*, 2007, **41**, 6129–6136.

16 W. A. Hall and M. V. Johnston, *J. Am. Soc. Mass Spectrom.*, 2012, **23**, 1097–1108.

17 K. Kristensen, T. Cui, H. Zhang, A. Gold, M. Glasius and J. D. Surratt, *Atmos. Chem. Phys.*, 2014, **14**, 4201–4218.

18 B. Witkowski and T. Gierczak, *Atmos. Environ.*, 2014, **95**, 59–70.

19 S. Lee and R. M. Kamens, *Atmos. Environ.*, 2005, **39**, 6822–6832.

20 B. Bonn, G. Schuster and G. K. Moortgat, *J. Phys. Chem. A*, 2002, **106**, 2869–2881.

21 J. W. DePalma, A. J. Horan, W. A. Hall and M. V. Johnston, *Phys. Chem. Chem. Phys.*, 2013, **15**, 6935–6944.

22 F. Yasmeen, R. Vermeylen, R. Szmigielski, Y. Iinuma, O. Boge, H. Herrmann, W. Maenhaut and M. Claeys, *Atmos. Chem. Phys.*, 2010, **10**, 9383–9392.

23 L. Muller, M. C. Reinnig, H. Hayen and T. Hoffmann, *Rapid Commun. Mass Spectrom.*, 2009, **23**, 971–979.

24 K. S. Docherty, W. Wu, Y. B. Lim and P. J. Ziemann, *Environ. Sci. Technol.*, 2005, **39**, 4049–4059.

25 P. J. Ziemann, *J. Phys. Chem. A*, 2003, **107**, 2048–2060.

26 M. Camredon, J. F. Hamilton, M. S. Alam, K. P. Wyche, T. Carr, I. R. White, P. S. Monks, A. R. Rickard and W. J. Bloss, *Atmos. Chem. Phys.*, 2010, **10**, 2893–2917.

27 M. Claeys, Y. Iinuma, R. Szmigielski, J. D. Surratt, F. Blockhuys, C. Van Alsenoy, O. Boge, B. Sierau, Y. Gomez-Gonzalez, R. Vermeylen, P. Van der Veken, M. Shahgholi, A. W. H. Chan, H. Herrmann, J. H. Seinfeld and W. Maenhaut, *Environ. Sci. Technol.*, 2009, **43**, 6976–6982.

28 T. Hoffmann, R. Bandur, U. Marggraf and M. Linscheid, *J. Geophys. Res.*, 1998, **103**, 25569–25578.

29 M. Ehn, E. Kleist, H. Junninen, T. Petaja, G. Lonn, S. Schobesberger, M. Dal Maso, A. Trimborn, M. Kulmala, D. R. Worsnop, A. Wahner, J. Wildt and T. F. Mentel, *Atmos. Chem. Phys.*, 2012, **12**, 5113–5127.

30 M. Ehn, J. A. Thornton, E. Kleist, M. Sipila, H. Junninen, I. Pullinen, M. Springer, F. Rubach, R. Tillmann, B. Lee, F. Lopez-Hilfiker, S. Andres, I. H. Acir, M. Rissanen, T. Jokinen, S. Schobesberger, J. Kangasluoma, J. Kontkanen, T. Nieminen, T. Kurten, L. B. Nielsen, S. Jorgensen, H. G. Kjaergaard, M. Canagaratna, M. Dal Maso, T. Berndt, T. Petaja, A. Wahner, V. M. Kerminen, M. Kulmala, D. R. Worsnop, J. Wildt and T. F. Mentel, *Nature*, 2014, **506**, 476–479.

31 J. Zhao, J. Ortega, M. Chen, P. H. McMurry and J. N. Smith, *Atmos. Chem. Phys.*, 2013, **13**, 7631–7644.

32 M. P. Rissanen, T. Kurten, M. Sipila, J. A. Thornton, O. Kausiala, O. Garmash, H. G. Kjaergaard, T. Petaja, D. R. Worsnop, M. Ehn and M. Kulmala, *J. Phys. Chem. A*, 2015, **119**, DOI: 10.1021/jp510966g.

33 L. Vereecken, J. F. Muller and J. Peeters, *Phys. Chem. Chem. Phys.*, 2007, **9**, 5241–5248.

34 J. D. Crounse, L. B. Nielsen, S. Jorgensen, H. G. Kjaergaard and P. O. Wennberg, *J. Phys. Chem. Lett.*, 2013, **4**, 3513–3520.

35 M. P. Rissanen, T. Kurten, M. Sipila, J. A. Thornton, J. Kangasluoma, N. Sarnela, H. Junninen, S. Jorgensen, S. Schallhart, M. K. Kajos, R. Taipale, M. Springer, T. F. Mentel, T. Ruuskanen, T. Petaja, D. R. Worsnop, H. G. Kjaergaard and M. Ehn, *J. Am. Chem. Soc.*, 2014, **136**, 15596–15606.
36 J. F. Pankow and W. E. Asher, *Atmos. Chem. Phys.*, 2008, **8**, 2773–2796.
37 B. Bonn and G. K. Moortgat, *Geophys. Res. Lett.*, 2003, **30**, DOI: 10.1029/2003GL017000.
38 C. Kidd, V. Perraud and B. J. Finlayson-Pitts, *Phys. Chem. Chem. Phys.*, 2014, **16**, 22706–22716.
39 P. M. Winkler, J. Ortega, T. Karl, L. Cappellin, H. R. Friedli, K. Barsanti, P. H. McMurry and J. N. Smith, *Geophys. Res. Lett.*, 2012, **39**, DOI: 10.1029/2012GL053253.
40 T. B. Nguyen, A. P. Bateman, D. L. Bones, S. A. Nizkorodov, J. Laskin and A. Laskin, *Atmos. Environ.*, 2010, **44**, 1032–1042.
41 S. Inomata, K. Sato, J. Hirokawa, Y. Sakamoto, H. Tanimoto, M. Okumura, S. Tohno and T. Imamura, *Atmos. Environ.*, 2014, **97**, 397–405.
42 A. Sadezky, P. Chaimbault, A. Mellouki, A. Rompp, R. Winterhalter, G. Le Bras and G. K. Moortgat, *Atmos. Chem. Phys.*, 2006, **6**, 5009–5024.
43 A. Sadezky, R. Winterhalter, B. Kanawati, A. Rompp, B. Spengler, A. Mellouki, G. L. Bras, P. Chaimbault and G. K. Moortgat, *Atmos. Chem. Phys.*, 2008, **8**, 2667–2699.
44 Y. Sakamoto, S. Inomata and J. Hirokawa, *J. Phys. Chem. A*, 2013, **117**, 12912–12921.
45 L. Vereecken, H. Harder and A. Novelli, *Phys. Chem. Chem. Phys.*, 2012, **14**, 14682–14695.
46 J. M. Anglada, S. Olivella and A. Sole, *Phys. Chem. Chem. Phys.*, 2013, **15**, 18921–18933.
47 M. Shiraiwa, M. Ammann, T. Koop and U. Poschl, *Proc. Natl. Acad. Sci. U. S. A.*, 2011, **108**, 11003–11008.
48 T. Koop, J. Bookhold, M. Shiraiwa and U. Poschl, *Phys. Chem. Chem. Phys.*, 2011, **13**, 19238–19255.
49 M. Shiraiwa and J. H. Seinfeld, *Geophys. Res. Lett.*, 2012, **39**, DOI: 10.1029/2012GL054008.
50 V. Perraud, E. A. Bruns, M. J. Ezell, S. N. Johnson, Y. Yu, M. L. Alexander, A. Zelenyuk, D. Imre, W. L. Chang, D. Dabdub, J. F. Pankow and B. J. Finlayson-Pitts, *Proc. Natl. Acad. Sci. U. S. A.*, 2012, **109**, 2836–2841.
51 D. L. Bones, J. P. Reid, D. M. Lienhard and U. K. Krieger, *Proc. Natl. Acad. Sci. U. S. A.*, 2012, **109**, 11613–11618.
52 L. Renbaum-Wolff, J. W. Grayson, A. P. Bateman, M. Kuwata, M. Sellier, B. J. Murray, J. E. Shilling, S. T. Martin and A. K. Bertram, *Proc. Natl. Acad. Sci. U. S. A.*, 2013, **110**, 8014–8019.
53 I. J. George and J. P. D. Abbatt, *Nat. Chem.*, 2010, **2**, 713–722.
54 C. Kidd, V. Perraud, L. M. Wingen and B. J. Finlayson-Pitts, *Proc. Natl. Acad. Sci. U. S. A.*, 2014, **111**, 7552–7557.
55 T. D. Vaden, D. Imre, J. Beranek, M. Shrivastava and A. Zelenyuk, *Proc. Natl. Acad. Sci. U. S. A.*, 2011, **108**, 2190–2195.
56 H. Lignell, M. L. Hinks and S. A. Nizkorodov, *Proc. Natl. Acad. Sci. U. S. A.*, 2014, **111**, 13780–13785.
57 J. J. Fritz and C. R. Fuget, *Ind. Eng. Chem.*, 1956, **1**, 10–12.
58 P. F. DeCarlo, J. R. Kimmel, A. Trimborn, M. J. Northway, J. T. Jayne, A. C. Aiken, M. Gonin, K. Fuhrer, T. Horvath, K. S. Docherty, D. R. Worsnop and J. L. Jimenez, *Anal. Chem.*, 2006, **78**, 8281–8289.
59 M. R. Canagaratna, J. L. Jimenez, J. H. Kroll, Q. Chen, S. H. Kessler, P. Massoli, L. Hildebrandt Ruiz, E. Fortner, L. R. Williams, K. R. Wilson, J. D. Surratt, N. M. Donahue, J. T. Jayne and D. R. Worsnop, *Atmos. Chem. Phys.*, 2015, **15**, 253–272.
60 P. F. DeCarlo, J. G. Slowik, D. R. Worsnop, P. Davidovits and J. L. Jimenez, *Aerosol Sci. Technol.*, 2004, **38**, 1185–1205.
61 J. D. Fenske, A. S. Hasson, S. E. Paulson, K. T. Kuwata, A. Ho and K. N. Houk, *J. Phys. Chem. A*, 2000, **104**, 7821–7833.
62 A. J. B. Cruicksh and A. J. B. Cutler, *J. Chem. Eng. Data*, 1967, **12**, 326–329.
63 S. Sarraute, I. Mokbel, M. F. C. Gomes, V. Majer and J. Jose, *Atmos. Environ.*, 2008, **42**, 4724–4734.
64 G. Koltzenburg, G. Behrens and D. Schultefrohlinde, *J. Am. Chem. Soc.*, 1982, **104**, 7311–7312.
65 J. J. Orlando and G. S. Tyndall, *J. Phys. Chem. A*, 2002, **106**, 312–319.
66 O. Welz, A. J. Eskola, L. Sheps, B. Rotavera, J. D. Savee, A. M. Scheer, D. L. Osborn, D. Lowe, A. M. Booth, P. Xiao, M. A. H. Khan, C. J. Percival, D. E. Shallcross and C. A. Taatjes, *Angew. Chem., Int. Ed.*, 2014, **53**, 4547–4550.
67 C. A. Taatjes, D. E. Shallcross and C. J. Percival, *Phys. Chem. Chem. Phys.*, 2014, **16**, 1704–1718.
68 L. Vereecken and J. S. Francisco, *Chem. Soc. Rev.*, 2012, **41**, 6259–6293.
69 H. J. Tobias and P. J. Ziemann, *Environ. Sci. Technol.*, 2000, **34**, 2105–2115.
70 M. Shiraiwa, L. D. Yee, K. A. Schilling, C. L. Loza, J. S. Craven, A. Zuend, P. J. Ziemann and J. H. Seinfeld, *Proc. Natl. Acad. Sci. U. S. A.*, 2013, **110**, 11746–11750.
71 K. Sato, S. Hatakeyama and T. Imamura, *J. Phys. Chem. A*, 2007, **111**, 9796–9808.
72 C. A. Taatjes, O. Welz, A. J. Eskola, J. D. Savee, A. M. Scheer, D. E. Shallcross, B. Rotavera, E. P. F. Lee, J. M. Dyke, D. K. W. Mok, D. L. Osborn and C. J. Percival, *Science*, 2013, **340**, 177–180.
73 S. Hatakeyama, H. Bandow, M. Okuda and H. Akimoto, *J. Phys. Chem.*, 1981, **85**, 2249–2254.
74 S. Hatakeyama and H. Akimoto, *Res. Chem. Intermed.*, 1994, **20**, 503–524.
75 O. Horie, P. Neeb, S. Limbach and G. K. Moortgat, *Geophys. Res. Lett.*, 1994, **21**, 1523–1526.
76 K. E. Leather, M. R. McGillen, M. C. Cooke, S. R. Utembe, A. T. Archibald, M. E. Jenkin, R. G. Derwent, D. E. Shallcross and C. J. Percival, *Atmos. Chem. Phys.*, 2012, **12**, 469–479.
77 S. Gab, E. Hellpointner, W. V. Turner and F. Korte, *Nature*, 1985, **316**, 535–536.
78 P. Neeb, F. Sauer, O. Horie and G. K. Moortgat, *Atmos. Environ.*, 1997, **31**, 1417–1423.
79 D. Huang, Z. M. Chen, Y. Zhao and H. Liang, *Atmos. Chem. Phys.*, 2013, **13**, 5671–5683.
80 P. Aplincourt and J. M. Anglada, *J. Phys. Chem. A*, 2003, **107**, 5812–5820.

81 J. E. Shilling, Q. Chen, S. M. King, T. Rosenoern, J. H. Kroll, D. R. Worsnop, P. F. DeCarlo, A. C. Aiken, D. Sueper, J. L. Jimenez and S. T. Martin, *Atmos. Chem. Phys.*, 2009, **9**, 771–782.

82 J. H. Kroll, J. D. Smith, D. L. Che, S. H. Kessler, D. R. Worsnop and K. R. Wilson, *Phys. Chem. Chem. Phys.*, 2009, **11**, 8005–8014.

83 G. Socrates, *Infrared and Raman characteristic group frequencies: tables and charts*, Wiley, Chichester, New York, 2001.

84 H. Kim, B. Barkey and S. E. Paulson, *J. Geophys. Res.*, 2010, **115**, DOI: 10.1029/2010JD014549.

85 A. T. Lambe, C. D. Cappa, P. Massoli, T. B. Onasch, S. D. Forestieri, A. T. Martin, M. J. Cummings, D. R. Croasdale, W. H. Brune, D. R. Worsnop and P. Davidovits, *Environ. Sci. Technol.*, 2013, **47**, 6349–6357.

86 N. J. Harrick, *Internal reflection spectroscopy*, Interscience Publishers, New York, 1967.

87 L. Yao, Y. Ma, L. Wang, J. Zheng, A. Khalizov, M. D. Chen, Y. Y. Zhou, L. Qi and F. P. Cui, *Atmos. Environ.*, 2014, **94**, 448–457.

88 M. Jaoui, K. G. Sexton and R. M. Kamens, *Atmos. Environ.*, 2004, **38**, 2709–2725.

89 R. Winterhalter, F. Herrmann, B. Kanawati, T. L. Nguyen, J. Peeters, L. Vereecken and G. K. Moortgat, *Phys. Chem. Chem. Phys.*, 2009, **11**, 4152–4172.

90 B. Barletta, S. Meinardi, F. S. Rowland, C. Y. Chan, X. M. Wang, S. C. Zou, L. Y. Chan and D. R. Blake, *Atmos. Environ.*, 2005, **39**, 5979–5990.

91 C. Warneke, J. A. de Gouw, J. S. Holloway, J. Peischl, T. B. Ryerson, E. Atlas, D. Blake, M. Trainer and D. D. Parrish, *J. Geophys. Res.*, 2012, **117**, DOI: 10.1029/2012JD017899.

92 J. J. Orlando and G. S. Tyndall, *Chem. Soc. Rev.*, 2012, **41**, 6294–6317.

93 M. Sipila, T. Jokinen, T. Berndt, S. Richters, R. Makkonen, N. M. Donahue, R. L. Mauldin, T. Kurten, P. Paasonen, N. Sarnela, M. Ehn, H. Junninen, M. P. Rissanen, J. Thornton, F. Stratmann, H. Herrmann, D. R. Worsnop, M. Kulmala, V. M. Kerminen and T. Petaja, *Atmos. Chem. Phys.*, 2014, **14**, 12143–12153.

94 O. Welz, J. D. Savee, D. L. Osborn, S. S. Vasu, C. J. Percival, D. E. Shallcross and C. A. Taatjes, *Science*, 2012, **335**, 204–207.

95 D. Stone, M. Blitz, L. Daubney, N. U. M. Howes and P. Seakins, *Phys. Chem. Chem. Phys.*, 2014, **16**, 1139–1149.

96 R. A. Cox and S. A. Penkett, *Nature*, 1971, **230**, 321–322.

97 R. L. Mauldin, T. Berndt, M. Sipila, P. Paasonen, T. Petaja, S. Kim, T. Kurten, F. Stratmann, V. M. Kerminen and M. Kulmala, *Nature*, 2012, **488**, 193–196.

98 R. Y. Zhang, A. Khalizov, L. Wang, M. Hu and W. Xu, *Chem. Rev.*, 2012, **112**, 1957–2011.

99 M. Kulmala, T. Petaja, M. Ehn, J. Thornton, M. Sipila, D. R. Worsnop and V. M. Kerminen, *Annu. Rev. Phys. Chem.*, 2014, **65**, 21–37.

